Bulletin of Earthquake Engineering
https://doi.org/10.1007/s10518-024-02071-z

REVIEW ARTICLE

Evaluating the performance of intensity prediction equations for the Italian area

Andrea Antonucci[1] · Giovanni Lanzano[1] · Andrea Rovida[1] · Sara Sgobba[1] · Vera D'Amico[2] · Augusto Antonio Gomez-Capera[1]

Received: 6 March 2024 / Accepted: 28 October 2024

Abstract
In this study, we evaluate the performance of five recent Intensity Prediction Equations (IPEs) valid for Italy comparing their predictions with intensities documented at Italian localities. We build four different testing datasets using the data contained in the most recent versions of the Italian Parametric Earthquake Catalogue CPTI15 and Macroseismic Database DBMI15 and we estimate the residuals between observed and predicted intensity values for all the selected IPEs. The results are then analyzed using a measure-oriented approach to score each model according to the goodness of model prediction and a diagnostic-oriented approach to investigate the trend of the residuals as a function of the different variables. The results indicate the capability of all the tested IPEs to reproduce the average decay of macroseismic intensity in Italy although with a general underestimation of high-intensity values. In addition, an in-depth investigation of the spatial and temporal patterns of the event residual term, computed using the best predictive model, is carried out. Lastly, we provide some hints for the selection of calibration datasets for the development of future intensity attenuation models.

Keywords Macroseismic intensity · Attenuation · Model scoring · Italy

1 Introduction

The entity of ground shaking generated by an earthquake that occurred in the pre-instrumental era is quantified through the earthquake effects documented at the local scale, i.e., the macroseismic intensity data points (hereafter IDPs). These latter represent a basic tool for several seismological analyses. For instance, the macroseismic data are of paramount importance for characterizing the earthquake parameters in the absence of instrumental recordings

✉ Andrea Antonucci
andrea.antonucci@ingv.it

[1] Istituto Nazionale di Geofisica e Vulcanologia, Via Alfonso Corti 12, Milano 20133, Italy

[2] Istituto Nazionale di Geofisica e Vulcanologia, Via Cesare Battisti 53, Pisa 20133, Italy

Published online: 21 November 2024

(e.g., Bakun and Wentworth 1997; Gasperini et al. 1999, 2010; Provost and Scotti 2020), needed for compiling long-term earthquake catalogs (e.g., Manchuel et al. 2018; Rovida et al. 2020, 2022a), and for testing and scoring probabilistic seismic hazard (PSH) assessments (e.g., Rey et al. 2018; D'Amico et al. 2024). Moreover, several efforts have been developed to provide PSH estimates in terms of macroseismic intensity using conventional approaches (e.g., Gomez-Capera 2006; Gomez-Capera et al. 2010; Cito et al. 2022) or the so-called site approach (Albarello and Mucciarelli 2002; D'Amico and Albarello 2008), both requiring the use of intensity prediction equations (IPEs), that model the decay of macroseismic intensity with the source-to-site distance. IPEs provide the expected median value and the associated standard deviation of ground shaking in terms of macroseismic intensity at a given site as a function of specific earthquake parameters (i.e., magnitude or epicentral intensity) and source-to-site distance. These models can also be applied to integrate the macroseismic intensity distribution of past earthquakes where documented effects are scarce (Antonucci et al. 2021; Oliveti et al. 2023) and to investigate the earthquake effects that could have been missed at a site (Antonucci et al. 2023). Due to the regional dependency of seismotectonic and attenuation properties, different approaches have been proposed for developing IPEs both at the local (e.g., Azzaro et al. 2006; 2016; Sørensen et al. 2009; 2010), national (e.g.Bakun and Scotti 2006; Pasolini et al. 2008a, b; Baumont et al. 2018; Bayrak et al. 2019), and wider scales (e.g., Stromeyer and Grunthal 2009; Bindi et al. 2011; Allen et al. 2012). Moreover, several functional forms have been used for developing IPEs. In detail, the attenuation models proposed in the literature are either logarithmic (e.g.Albarello and D'Amico 2004; Pasolini et al. 2008b; Musson 2013; Tosi et al. 2015) or non-logarithmic (e.g., Gasperini 2001; Gomez-Capera 2006). The former models consider macroseismic intensity to be proportional to the logarithm of the energy released by an earthquake, assuming that the energy of seismic waves decays as a function of geometrical spreading and anelastic dissipation, whereas the latter models derive from a statistical approach that allows the best fitting of macroseismic data. In Italy, a long tradition of historical investigations of past earthquakes has produced a large amount of macroseismic data that has greatly improved the seismological knowledge of the territory. In particular, the data contained in the latest version of the Italian Macroseismic Database (Database Macrosismico Italiano - DBMI15; Locati et al. 2022) and the Italian Parametric Earthquake Catalogue (Catalogo Parametrico dei Terremoti Italiani - CPTI15; Rovida et al. 2020, 2022b) have considerably increased compared to those included in their previous versions. This has allowed the development of several intensity attenuation models for Italy and their continuous updating, as well as studies aimed at testing their performance (Albarello and D'Amico 2005; Mak et al. 2015).

In this work, we focus on the most recent IPEs developed for Italy (Rovida et al. 2020; Gomez-Capera et al. 2024; Lolli et al. 2024), that are specifically calibrated with the most recent data of shallow crustal earthquakes using moment magnitude as the earthquake size parameter. We do not take into account IPEs developed for the volcanic areas (e.g., Azzaro et al. 2023) because the attenuation features of these zones are different from the rest of Italy, and the model developed with intensities assessed from web questionnaires (Tosi et al. 2015) because it is calibrated with local magnitude (M_L) and data not included in DBMI15. The main scope of this research is to identify the best predictive model for Italy through an in-depth analysis. In detail, we evaluate the performance of the most recent attenuation models by comparing the documented intensity data contained in DBMI15 with the

Table 1 Reference, functional form, standard deviation (σ), regression coefficients (a-d), and pseudo focal depth (h) of the selected IPEs. ID is the identifier used in this study

ID	Reference	Functional Form	σ	a	b	c	d	h
ROV20	Rovida et al. 2020	Equations [1–2]	0.76*	-1.227	0.0029	1.248	1.537	7.45
LOL24all	Lolli et al. 2024	Equations [1–2]	0.83*	-2.578	0.0081	1.072	1.867	4.49
LOL24ins	Lolli et al. 2024	Equations [1–2]	0.82*	-1.459	0.0066	1.235	1.610	6.35
GOM24	Gomez-Capera et al. 2024	Equation [4]	0.748	1.8117	0.0039	2.61	1.42	9.87
GOM24crv	Gomez-Capera et al. 2024	Equation [5b]	0.731	0.0320	0.0030	0.19	1.36	8.72

*Obtained by summing the two relevant variances estimated for Eq. (1) and Eq. (2)

Table 2 Summaries of calibration dataset used in each selected IPE

ID	*N*° Events	Time range	Mw range	Focal Depth	*N*° IDPs	Int range
ROV20	354	1903–2013	2.7–7.1	<30 km	30,138	2–11
LOL24all	744	1200–2017	*	*	33,038	3–11
LOL24ins	338	1904–2017	*	*	20,029	3–11
GOM24	119	1908–2013	3.8–7.1	<35 km	16,260	3–11
GOM24crv	119	1908–2013	3.8–7.1	<35 km	16,260	3–11

* Data not provided in the original paper

predicted values computed through the considered IPEs from the epicentral parameters collected in CPTI15. We analyze the results in order to highlight possible limitations in the prediction of earthquake effects as a function of different variables. The paper is structured as follows: (i) description of the selected IPEs and of the four testing datasets used; (ii) methodology of analysis in terms of differences between documented and predicted intensity values (analysis of the residuals) and statistical method adopted for defining the best predictive model; (iii) results derived from all the considered IPEs with a discussion of those obtained with the best predictive model.

2 IPEs selected for the evaluation

We select the attenuation models following Mak et al. (2015) who apply to IPEs the criteria proposed by Cotton et al. (2006) for selecting Ground-Motion models (GMMs). In this perspective, we take into account the differences between macroseismic data, which are ordinal, discrete, and range-limited values, and ground motion measurements which are continuous variables. This also implies that macroseismic data are normally distributed whereas ground motion data are log-normally distributed. Despite this, the similarity of several seismological applications that use these data (i.e., seismic hazard analysis, shaking scenarios, etc.) allows us to consider the criteria adopted for selecting GMMs appropriate for IPEs, too. With the aim of evaluating the performance of the most recent Italian IPEs, i.e., their ability to predict the intensity value at a given site as a function of earthquake moment magnitude and source-to-site distance, we select the attenuation models proposed by: (i) Rovida et al. (2020); (ii) Lolli et al. (2024); and (iii) Gomez-Capera et al. (2024), summarized in Tables 1 and 2. The IPE proposed by Rotondi et al. (2016, 2019) is not included in the analysis because it is based on a non-parametric approach and estimates the probability of the intensity at the site adopting a binomial distribution as a function of epicentral intensity and distance; therefore its predictions are not directly comparable with those of the selected IPEs that predict an intensity value as a function of moment magnitude. The selected IPEs are based on a log-linear standard model (e.g., Kövesligethy 1907; Gupta and Nuttli 1976) with the linear distance term accounting for the anelastic dissipation and the logarithmic distance term accounting for the geometrical spreading. In addition, the selected models describe macroseismic intensity attenuation as a function of the epicentral distance (i.e., the distance between the site location and the epicenter of the earthquake), and they do not consider the actual rupture plane or its surface projection. Lolli et al. (2024) proposed two models, hereafter LOL24all and LOL24ins; these models represent an update of the widely used IPE for the Italian area published by Pasolini et al. (2008b). In addition, Rovida et al. (2020), hereafter ROV20, calibrated the coefficients of Pasolini et al. (2008b) to be used for calculating the macroseismic parameters in the CPTI15.

In detail, the functional form adopted in ROV20, LOL24all, and LOL24ins to predict the intensity I at a given site from the I_E value (defined as the average expected intensity at the epicenter) is:

$$I = I_E - b * (D - h) - c * [ln\ (D)\ - ln\ (h)] \tag{1}$$

$$I_E = a + d * M_w \tag{2}$$

where M_w is the moment magnitude, and D is the pseudo hypocentral distance (in km) estimated from epicentral distance (R) and pseudo focal depth (h) as:

$$D\ = \sqrt{R^2 + h^2} \tag{3}$$

The ROV20, LOL24all, and LOL24ins models are calibrated with a two-step regression analysis. In the first step, the intensity attenuation with hypocentral distance is correlated with the intensity expected at the epicenter I_E. In the second step, the parameter I_E is correlated with magnitude using an error-in-variable (EIV) method following the procedure described in Fuller (1987) and applied by Castellaro et al. (2006). The main differences among the ROV20, LOL24all, and LOL24ins models derive from the data selection used for their calibration (see Table 2). LOL24all and LOL24ins consider the data collected in the CPTI15 and DBMI15 for earthquakes with more than 10 IDPs. Moreover, the authors applied to the calibration dataset quality criteria related to possible incompleteness of low intensities excluding from the dataset all the intensity data less than 3 MCS (Mercalli-Cancani-Sieberg; Sieberg 1923) and data located at epicentral distances where an average intensity lower than 4 MCS is expected according to a preliminary attenuation function (see Lolli et al. 2024 for details). LOL24all was calibrated using 33,038 intensity data related to 744 Italian earthquakes that occurred after 1200 C.E., whereas LOL24ins took into account 338 earthquakes with only instrumental magnitude that occurred after 1904 and the corresponding 20,029 intensity data. The coefficients of the ROV20 model were obtained from the same dataset used for calibrating the Boxer algorithm (Gasperini et al. 2010) adopted for estimating the earthquake parameters of CPTI15. In particular, the calibration dataset is made of 354 earthquakes with instrumental moment magnitudes between 2.8 and 7.1 that occurred in the period 1903–2013 for a total of 30,138 IDPs from DBMI15 with intensity ranging from 2 to 11 MCS. The earthquakes deeper than 30 km and with less than 10 IDPs were excluded from the dataset.

Gomez-Capera et al. (2024) developed several IPEs based on two functional forms. The authors then compared and tested the obtained IPEs through a sensitivity analysis of the calibrated coefficients and a validation process based on a residual analysis, identifying the two best-performing IPEs that are selected in this study (hereafter GOM24 and GOM-24crv). These two attenuation models are derived from those developed by Howell and Schultz (1975) and are based on an empirical relationship between macroseismic intensity and seismic energy. The functional form of GOM24 is a classical log-linear attenuation model as a function of epicentral distance (*R*) and moment magnitude (M_w):

$$I = a - b * D - c * Log\left(D\right) + d * M_w \tag{4}$$

GOM24crv is an alternative linear functional form in which the logarithm of macroseismic intensity increases with M_w in the logarithmic form:

$$I = a - b\ *\ D -\ c\ *\ Log\left(D\right) + d\ * LogM_w \tag{5a}$$

This equation is equivalent to:

$$I = 10^a * 10^{-bD} *\ D^{-c} * {M_w}^d \tag{5b}$$

D represents the pseudo hypocentral distance and is estimated through Eq. (3). Unlike other models, GOM24 and GOM24crv adopt a non-linear least squares regression for determining the four coefficients (*a*-*d*) and the pseudo focal depth (*h*). The calibration dataset consists of 16,260 IDPs collected in DBMI15 related to 119 earthquakes of CPTI15 with reliable instrumental Mw in the range 3.8–7.1, that occurred in the period 1908–2013. The events with focal depth > 35 km are not used in the calibration dataset. In addition, macroseismic intensities < 3 MCS are excluded due to a possible incompleteness of the data. All the selected IPEs do not consider in their calibration dataset the earthquakes that occurred in the Italian volcanic regions (i.e., Mt. Etna, Aeolian islands, and Campanian volcanoes) and those with the epicenter located at sea. The coefficient *a* is calibrated to reflect the boundary conditions of the source, *b* is associated with the anelastic attenuation, *c* and *d* define the rate of energy geometrical spreading and the dependence of the magnitude, respectively (Table 1). Table 1 reports the standard deviation (σ) of each model. In particular, the σ of GOM24 and GOM24crv derives from the root mean square of the residuals (difference between observed and predicted macroseismic intensity at sites) of the calibration dataset. The LOL24ins, LOL24all, and ROV20 models provide two independent values of σ that are obtained from the two-step regression analysis (Eq. 1 and Eq. 2; see values listed in Tables 1 and 2 in Lolli et al. 2024). For those models, the total standard errors of the separate regressions are computed following the usual error law, that is by summing the two relevant variances (Pasolini et al. 2008b).

As a comparison of the five tested models, Fig. 1 shows the decay of macroseismic intensity as a function of the epicentral distance (*R*) according to the selected IPEs for moment magnitude 5.0 (Fig. 1a) and 6.5 (Fig. 1b). For predictions of $M_w = 5.0$ at distances lower than 10 km, all the selected IPEs provide similar intensity values, i.e., between intensity 6

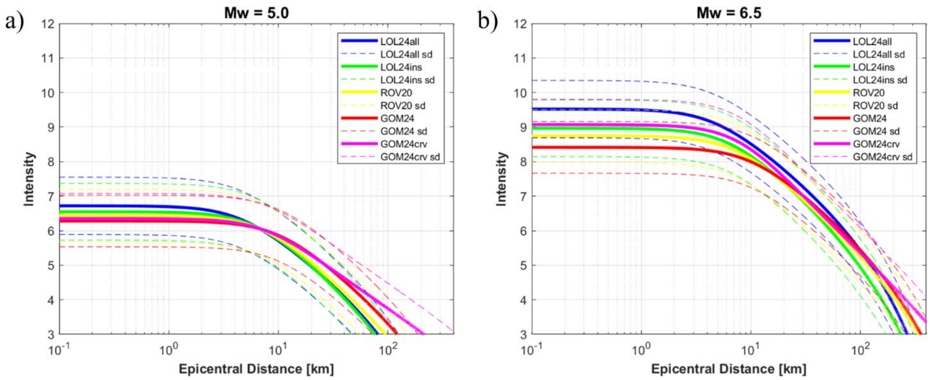

Fig. 1 Decay of macroseismic intensity as a function of the epicentral distance for the selected IPEs for moment magnitude 5.0 **a** and 6.5 **b**. The dotted lines represent the standard deviation of the models

and 7 MCS; at higher distances, GOM24crv shows a decay of intensity with distance slower than the other four models, among which LOL24ins and LOL24all show the fastest decay. Considering $M_w = 6.5$ (Fig. 1b), there is quite a large variability of the predictions in near-source conditions ($R < 5$ km), where the LOL24all model predicts an intensity of 9–10 MCS, whereas GOM24 predictions are between 8 and 9 MCS.

3 Testing datasets

To test the performance of the selected IPEs, we consider four datasets derived from the most recent version of CPTI15 (Rovida et al. 2022b) and DBMI15 (Locati et al. 2022), according to specific criteria: two datasets (hereafter Dataset #1 and Dataset #1alt)include only earthquakes with instrumentally determined magnitude and location, occurred between 1907 and 2020; the other two datasets (hereafter Dataset #2 and Dataset #2alt) contain both historical and recent earthquakes with parameters derived only from macroseismic data, occurred in the period 1117–1978 (see Rovida et al. (2020) for details). The earthquakes of the four datasets are selected taking into account the following common criteria:

- Number of associated IDPs ≥ 10;
- Moment magnitude Mw ≥ 4.0;
- Hypocentral depth ≤ 30 km (historical events without depth assessment are considered within this range);
- Inland epicenter;
- Mainshocks as identified with the method of Gardner and Knopoff (1974), following Meletti et al. (2021).

In addition, earthquakes in the Italian volcanic areas (Mt. Etna, Aeolian islands, and Campanian volcanoes) and of the Calabrian Arc subduction zone are discarded because of their peculiar attenuation features. Also, earthquakes with intensity data derived from the French database SisFrance (BRGM-EDF-SisFrance 2014) are not considered.

As for the selection of IDPs, we adopt specific selection criteria. In order to minimize the influence of the incompleteness of the macroseismic data, we exclude from the Dataset #1 and Dataset #2 the data with macroseismic intensity < 4 MCS and those located at epicentral distance > 200 km (see Fig. 2a and 2 b). This is because despite the significant number of IDPs with low intensities due to the inclusion of many moderate energy earthquakes in the DBMI15, the IDPs < 4 are still small in number compared to those of intensity ≥ 4 see figure 3 of another article (Locati et al.2022) and the macroseismic intensity distributions of several earthquakes cover the territory within 200 km.

A different way of accounting for the incompleteness of macroseismic data, particularly for low intensities, is proposed by Pasolini et al. (2008b) and Lolli et al. (2024). Following their criteria, we build two alternative datasets (i.e., Dataset #1alt and Dataset #2alt) to further test the selected IPEs. To this purpose, these two alternative datasets consider all the intensity data except those with intensity ≤ 2 MCS and discard the data located at epicentral distances where an intensity lower than 4 is expected (see Fig. 2c and 2d) based on an attenuation function proposed by Pasolini et al. (2008b).Moreover, intensities not expressed

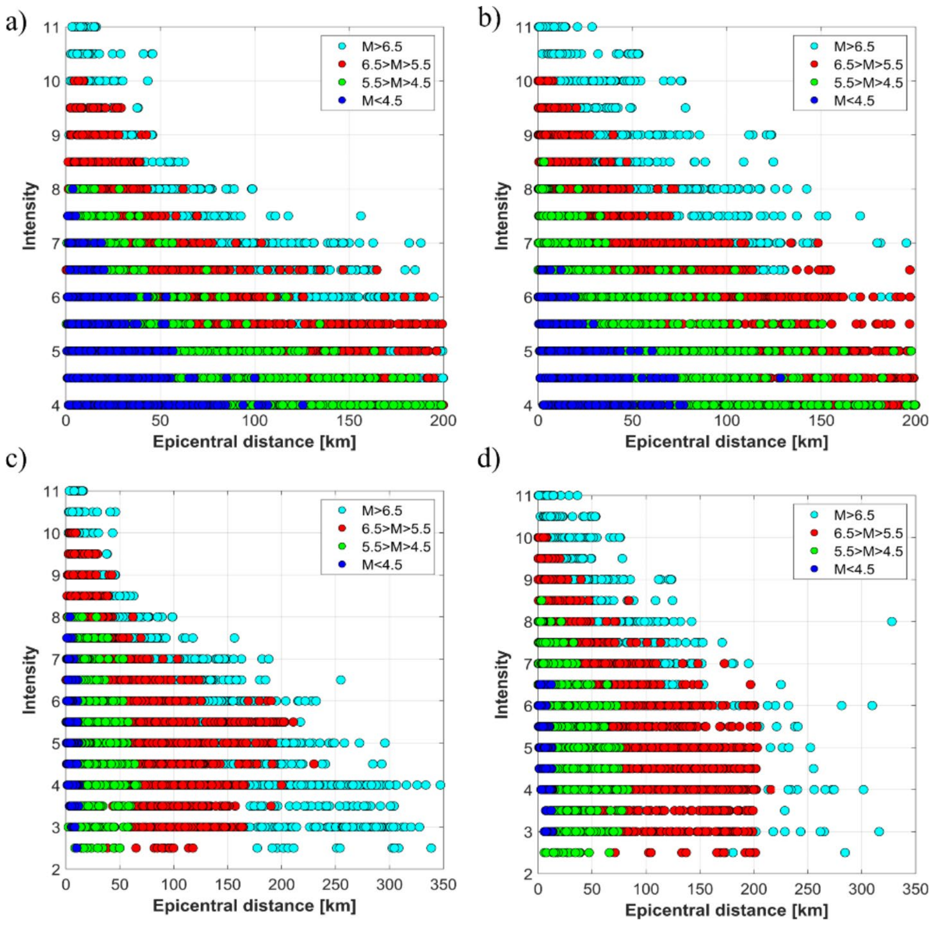

Fig. 2 Intensity versus epicentral distance of macroseismic data contained in Dataset #1 **a**, Dataset #2 **b**, Dataset #1alt **c**, and Dataset #2alt **d** according to earthquake magnitude ranges

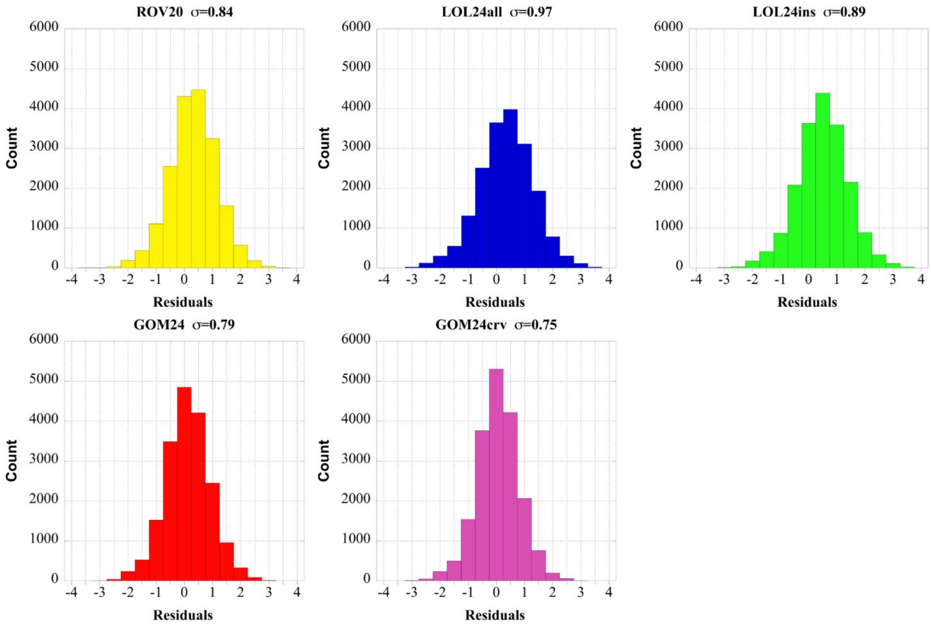

Fig. 3 Total residuals R_{es} (Eq. 6) of Dataset #1 versus instrumental moment magnitude for the IPEs in Table 1

with numerical values in DBMI15 (e.g., "F" for felt, "D" for generic damage, and so on; see Rovida et al. 2020) are discarded from all datasets.

As a result, Dataset #1 contains 18,714 IDPs with intensity up to 11 MCS, related to 213 earthquakes with instrumental Mw between 4.0 and 7.1 whereas Dataset #1alt includes 12,900 IDPs for 196 earthquakes. Dataset #2 is composed of 13,998 IDPs with intensity up to 11 MCS, related to 357 earthquakes with Mw between 4.0 and 7.3 derived from macroseismic data and Dataset #2alt contains 12,065 IDPs related to 352 events. We are aware that some events in the testing datasets may be included in the calibration datasets of the selected models. However, the possible overfitting effects due to the partial overlap between the testing and calibration datasets would be common to all the considered IPEs.

The events selected for all the datasets are provided in Online Resource 3 (Table S1).

4 Residual analysis and ranking methods

The total residual R_{es} can be calculated as the difference between the macroseismic intensity observations MI_{obs} (from the selected datasets) and the predictions at the same sites MI_{pred} of the models given in Table 1, as:

$$R_{es} = MI_{obs} - MI_{pred} \tag{6}$$

According to the simplest scheme for residual decomposition (Al Atik et al. 2010), the total term can be separated into:

$$R_{es} = \delta\, B_e \,+\, \delta\, W_{es} \tag{7}$$

where δB_e is the between-event and δW_{es} is the within-event related to the event *e* and the site *s*. Generally, in applications related to GMMs, these are random terms estimated with mixed-effects regression approaches to ensure robust estimation of random effects even for datasets with unbalanced numbers of observations for each random variable (Stafford 2014). In this case, the between-event is calculated simply as the mean of the residuals for the specific event *e*:

$$\delta\, B_e = \frac{1}{N_e}\sum\nolimits_{i=1}^{N_e} R_{es} \tag{8}$$

where N_e is the number of IDPs per event, which is always greater than or equal to 10 (see previous section). From a physical point of view, the between-event is the average misfit of observations of one particular earthquake with respect to the median IPE prediction. In addition, δBe represents the event-term and can be attributed to differences in regional source characteristics in terms of parameters that influence the level of ground motion. Conversely, the within-event is the residual error, obtained as:

$$\delta\, W_{es} = R_{es} -\ \delta\, B_e \tag{9}$$

δW_{es} represents the aleatory error, which is not related to event or source effects but can be attributed to other features not introduced into the original model, such as site or propagation effects.

According to Mak et al. (2015), we evaluate the performance of the data-driven models using the total residuals and following two complementary approaches: the first is measure-oriented and uses a score to describe the overall goodness of fit between model predictions and actual observations. However, the scoring (or ranking) methods do not indicate which part of a model performs well or badly. The second one is the diagnostic-oriented approach, which qualitatively evaluates the performance of the models for different input scenarios.

Concerning the first measure-oriented approach, we adopt two metrics to evaluate the performance of the predictive models: (i) the log-likelihood (LLH), which is an index, proposed for the first time by Scherbaum et al. (2009) in the framework of PSH assessment for Europe (Delavaud et al. 2012), to rank both IPEs and GMMs; (ii) the mean absolute error (MAE), introduced by Mak et al. (2015) for validating Italian IPEs.

Scherbaum et al. (2009) derived this selection procedure from an information-theoretic perspective, where the distance between the unknown model, representing the reality, and the candidate model is measured, employing the concept of likelihood for a set of observations. Let us assume that we want to measure the likelihood of a model, described by a continuous probability density function *g(x)*, given the set of independent observations $x = \{xi\}$ with $i = 1 \ldots N$. The log-likelihood of the model, given the sample set *x*, is:

$$log_b L\,(x) = \frac{1}{N}\sum\nolimits_{i=1}^{N} log_b\,(g(\,x_i) \tag{10}$$

where N is the number of observations and the logarithm base b is 2. The higher the value of LLH (closer to zero), the better the performance of the model. Despite some issues related to this performance index, raised by some authors in the last decade (Kale and Akkar 2013; Arroyo et al. 2014), it is still the most popular method to evaluate the performance of a model.

As widely detailed by Mak et al. (2015), another methodology to evaluate the goodness of a model in reproducing the observed intensity data is represented by the mean absolute error (MAE). The MAE for each earthquake, named MAE_e, is defined as:

$$MAE_e = \frac{1}{N_e}\sum_{i=1}^{N_e}|MI_{obs} - MI_{pred}| = \frac{1}{N_e}\sum_{i=1}^{N_e}|R_{es}| \tag{11}$$

where N_e is the number of IDPs for each event. Note that MAE_e is different from δBe in Eq. (8) since the total residuals are considered in absolute values. In order to obtain a unique indicator for evaluating the performance of each selected IPE, the final MAE is computed as the average value of all the MAE_e. The closer to zero the MAE value, the better the performance of the model. Moreover, to follow the diagnostic-oriented approach as well, we investigate the trend of the residuals as a function of the explanatory variables and predicted intensity values, as a complement to the ranking results.

5 Results

5.1 Analysis of residuals' trends and statistics

Since the residuals of the models as defined in Eq. (6) are zero-mean Gaussian processes, we make some statistical tests of normality to assess the model performance. Table 3 shows, for each selected IPE, the main statistical indexes of the distribution of the total residuals, such as the minimum, maximum, and median value, the standard deviation, the skewness, the kurtosis, the LLH value of Eq. (10), and the MAE value for the selected testing datasets. In the following, there are some figures showing the trend of the residuals for Dataset #1; the corresponding figures for the other three datasets are provided in Online Resource 1.

Figure 3 shows the histograms of the residuals for each model considered in our analysis over Dataset #1. All models exhibit a positive bias (see median values in Table 3), in some cases very small (e.g., GOM24crv) and in other cases slightly larger (e.g., LOL24ins). Figure 3 also shows that the residuals are not centered on mean zero for ROV20, LOL24all, and LOL24ins, indicating an overall slight to moderate underestimation of empirical data for the models considered. Similar observations can be made for Dataset #2 (see Fig. S1) and Dataset #2alt (see Fig. S9), whereas Dataset #1alt shows a negative bias except for the LOL24ins and ROV20 models (see Table 3 and Fig. S5).

Since the Skewness is a measure of the lack of symmetry with respect to a normal distribution, all the models show values close to zero, lower than 0.2 in absolute values for all the datasets, indicating very small asymmetries of the residuals' distributions. Kurtosis is instead a measure of whether the data are heavy- or light-tailed with respect to a normal distribution: also in this case the model residual distributions do not have many outliers and therefore are not particularly long-tailed.

Table 3 Statistical indexes of the total residuals for each selected IPE

Model	Min	Max	Median	Sd	Skewness	Kurtosis	LLH	MAE
Dataset 1								
ROV20	-3.44	3.49	0.33	0.84	-0.10	0.34	-1.9354	0.68703
LOL24all	-3.74	3.93	0.36	0.97	-0.14	0.30	-2.1559	0.84079
LOL24ins	-3.50	3.80	0.50	0.89	-0.10	0.39	-2.1497	0.77587
GOM24	-3.39	3.30	0.11	0.79	-0.02	0.37	-1.7359	0.59162
GOM24crv	-3.60	3.41	0.06	0.75	-0.08	0.71	-1.6406	0.54648
Dataset 2								
ROV20	-3.19	4.00	0.31	0.83	-0.02	0.27	-1.9100	0.66541
LOL24all	-3.87	3.65	0.20	0.88	-0.09	0.39	-1.9031	0.70404
LOL24ins	-3.36	4.17	0.39	0.88	0.03	0.26	-2.0456	0.71947
GOM24	-2.96	3.86	0.20	0.82	0.04	0.20	-1.8264	0.62725
GOM24crv	-3.63	4.01	0.11	0.80	0.06	0.51	-1.7619	0.58010
Dataset 1alt								
ROV20	-3.75	3.38	0.00	0.87	-0.06	0.21	-1.8729	0.64780
LOL24all	-4.00	3.10	-0.10	0.89	-0.13	0.40	-1.9054	0.65226
LOL24ins	-3.74	3.50	0.17	0.89	-0.15	0.23	-1.9119	0.65433
GOM24	-3.83	3.30	-0.15	0.87	0.01	0.21	-1.8980	0.66409
GOM24crv	-3.88	3.41	-0.17	0.87	-0.02	0.16	-1.9314	0.65431
Dataset 2alt								
ROV20	-4.24	4.02	0.19	0.91	-0.12	0.21	-1.9944	0.66534
LOL24all	-4.41	4.62	0.01	0.89	-0.17	0.31	-1.8707	0.63980
LOL24ins	-4.31	5.09	0.24	0.93	-0.05	0.24	-2.0194	0.66691
GOM24	-4.14	3.99	0.14	0.93	-0.15	0.16	-2.0294	0.68601
GOM24crv	-4.26	4.01	0.07	0.94	-0.12	0.25	-2.0261	0.66474

Figure Firegu 4 shows the trend of the residuals with epicentral distance: the models generally tend to underestimate observations at long distances (> 100 km ca.)and overestimate those at short distances. In particular, the ROV20, LOL24all, and LOL24ins models show a distance scaling that does not reproduce the empirical data in Dataset #1, with an underestimation of observed intensity increasing with epicentral distances greater than 30 km ca. This may be because the datasets used for calibrating the models of Lolli et al. (2024) apply data selection criteria related to possible incompleteness of data at long distances (see Sect. 2). Indeed, considering Dataset #1alt which takes into account these criteria, the underestimation of observed intensity at long epicentral distances is not shown, except a slight one for LOL24ins (see Fig. S6). Dataset #2 and Dataset #2alt (see Fig. S2 and Fig. S10 show a slight underprediction of observed intensity at distances close to the epicenter. This trend is less appreciable for the LOL24all model.

Figure 5 shows the trend of the residuals as a function of the other explanatory variable, i.e., the moment magnitude, considering 0.2 M_w bins: all models tend to underestimate the empirical data of Dataset #1 for low magnitudes (M_w<5 circa), and this trend is more evident for the ROV20, LOL24all, and LOL24ins. The trend observed for $M_w \geq 6$ is very similar for all the considered models, with a general overestimation of empirical data, in particular for magnitude ranging from 6.0 to 6.5. This trend is not confirmed for Dataset #2 and Dataset #2alt where all the selected models show a good performance with an average residual in the range of ± 1 intensity value (see Fig. S3; S11), which is in agreement with the uncertainty associated with the definition of macroseismic intensity (ordinal and discrete).

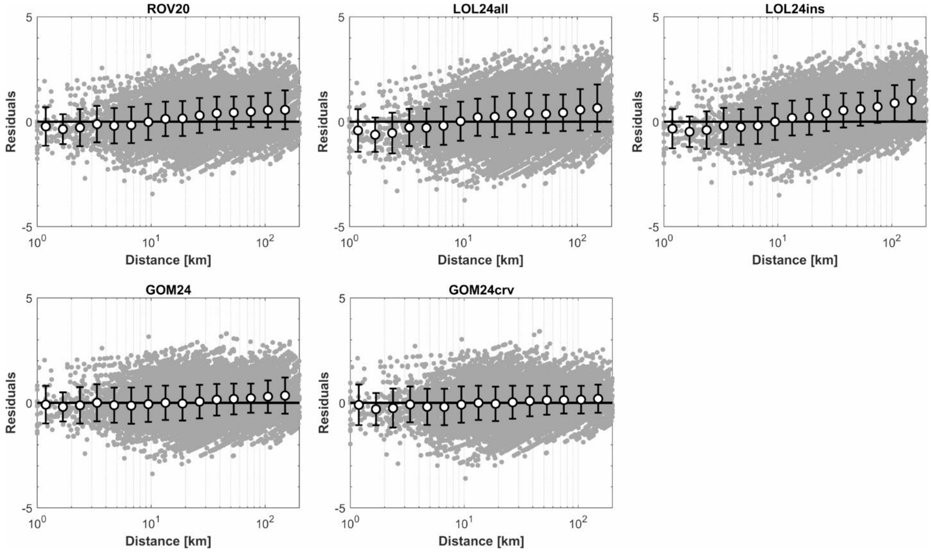

Fig. 4 Histograms of total residuals R_{es} (Eq. 6) of Dataset #1 for the IPEs in Table 1

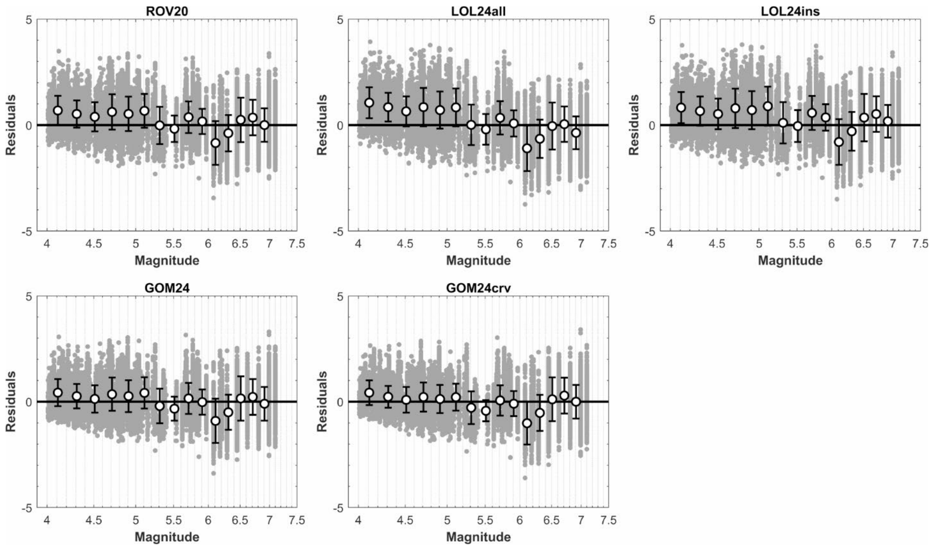

Fig. 5 Total residuals R_{es} (Eq. 6) of Dataset #1 versus epicentral distance for the IPEs in Table 1

The underestimation of data for low magnitudes is not shown for Dataset #1alt (see Fig. S7), whereas the trend for high M_w values is similar to that observed for Dataset #1.

Finally, Fig. 6 shows the trend of the residuals as a function of predicted intensity values for Dataset #1. In all the cases, there is a large variability in the residuals for predicted intensity ≤ 8 MCS, probably due to the high number of data in these intensity classes. However, the average residuals calculated are within ± 1 for all the selected models. Figure 6 also shows all the IPEs tend to underestimate the observed data for low-intensity values (i.e. $MI_{pred} < 5$) whereas the ROV20 and GOM24 models do not predict intensities > 9, and underestimate these intensities for the considered earthquakes. In addition, the LOL24all and GOM24crv models reproduce high-intensity data better than the LOL24ins model, with the average residuals for $MI_{pred} > 9$ very close to zero. The LOL24all and GOM24crv models perform better than the others with Dataset #2 and Dataset #2alt (see Fig. S4; S12).

5.2 Selection of the best-performing model

For the purpose of objectively formulating a preference for a single model on the basis of the two different adopted scoring techniques, we follow the strategy proposed by Lanzano et al. (2020) for GMMs: since the tested models exhibit scores that could differ by a few centesimal points, we compute an ordinal score for each scoring metric and testing dataset, accounting for their cardinality. In particular, we assign 5 points to the best-performing IPE (LLH or MAE values closest to zero) and 1 point to the worst, based on the scoring results in Table 3. The ordinal total score for each model is then obtained from the sum of the scores for each scoring metric and dataset. Table 4 provides the partial and total scores of each IPE for all the datasets.

On the basis of the measure-oriented approach, the best-performing model is GOM24crv, which totals 30 points. This result is also confirmed by the diagnostic-oriented approach since GOM24crv exhibits an almost zero-mean trend as a function of both distance and magnitude (see Figs. 5 and 3, and 6). The only caveat concerns the results obtained for the two alternative datasets (i.e., Dataset #1alt and Dataset #2alt) where the GOM24crv shows good performance according to the MAE score but not to the LLH one. The runner-up is the ROV20 model, followed by LOL24all, GOM24, and LOL24ins.

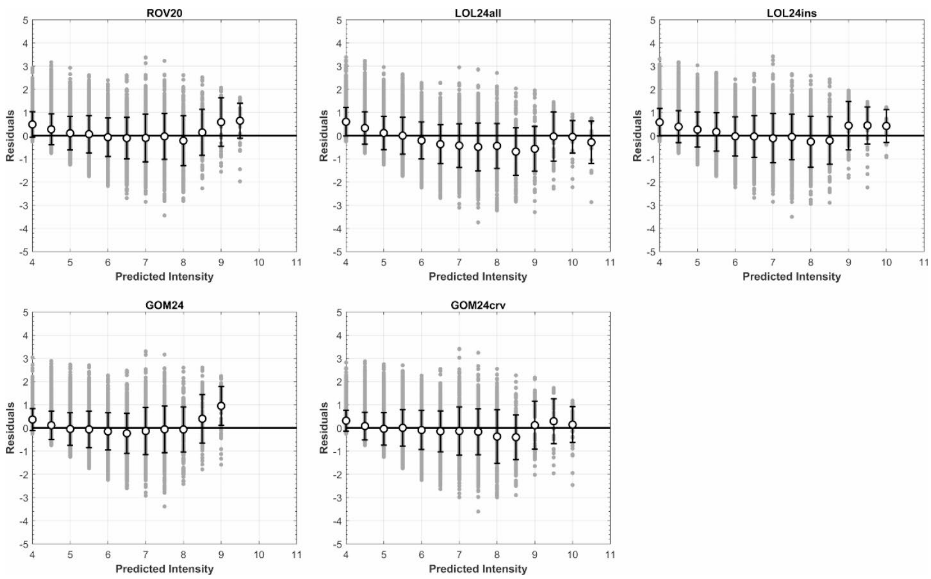

Fig. 6 Total residuals R_{es} (Eq. 6) of Dataset #1 versus predicted intensities for the IPEs in Table 1

Table 4 Partial and total score of the selected IPEs

Model	LLH scoring				MAE scoring				Total score
	D #1	D #2	D #1alt	D #2alt	D #1	D #2	D #1alt	D #2alt	
ROV20	3	2	5	4	3	3	5	3	28
LOL24all	1	3	3	5	1	2	4	5	24
LOL24ins	2	1	2	3	2	1	2	2	15
GOM24	4	4	4	1	4	4	1	1	23
GOM24crv	5	5	1	2	5	5	3	4	30

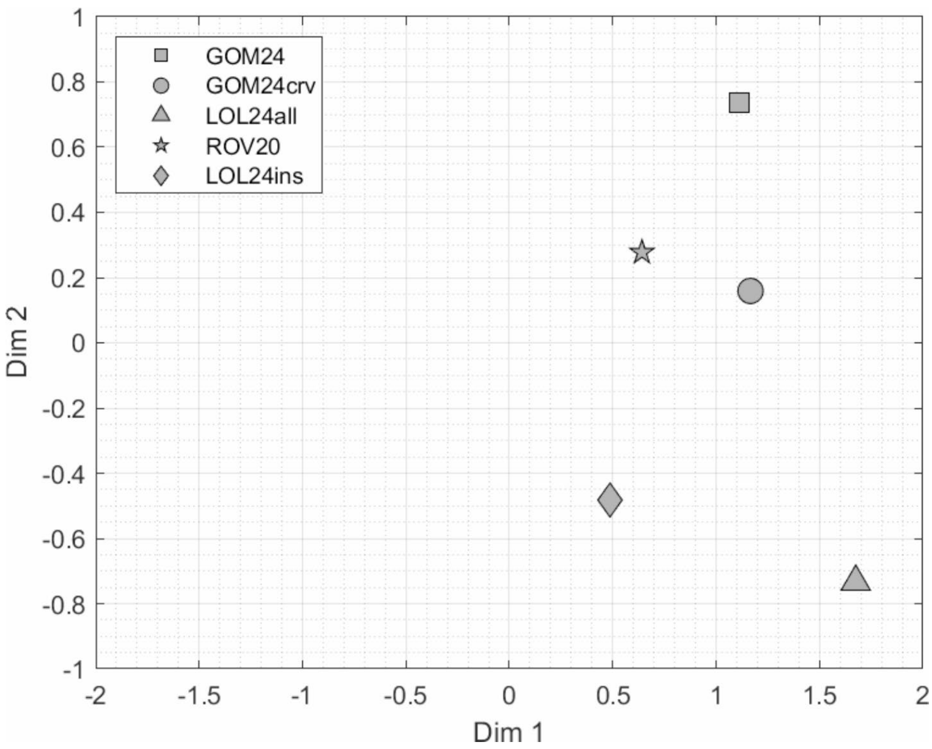

Fig. 7 Sammon's maps of the selected IPEs

We also employ the Sammon maps (Fig. 7), which allow mapping a high-dimensional space (i.e., the number of explanatory variables of the model) to a space of lower dimensionality (2D), by trying to preserve the structure of inter-point distances. The Sammon map, originally proposed by Sammon (1969), is particularly useful for visualizing and interpreting different datasets and models and is commonly used in ground motion modeling to visually compare GMMs from different predictive parameters (magnitude and distance) in single plots (Scherbaum et al. 2010; Goulet et al. 2017; Drouet et al. 2020; Aldama-Bustos et al. 2023; among others). We represent the selected IPEs on Sammon's space (see Fig. 7) by dividing the map into a grid of squares to show median predictions for various magnitudes and distances. We consider earthquake magnitudes between Mw 4.5 and 6.5 with a step of 0.5, and distances between 0 and 200 km with a step of 20. This approach allows us to visually compare median predictions and assess how close the IPEs are in predicting similar intensity levels. In Fig. 7, we observe that the points in two dimensions cover a wide range of the intensity prediction space, and we do not see any overlapping or clusters. This suggests that there are significant variations in the predictions of the considered IPEs, despite the similarity in functional formsso we are dealing with non-redundant models.

5.3 Spatial and temporal patterns of the best predictive model

In this section, we search for spatial and temporal patterns of the between-events δBe (Eq. 8) of the best predictive model, identified above as GOM24crv. Being Dataset#1alt and Dataset #2alt a subset of the earthquake contained in Dataset #1 and Dataset #2 that cut-away many observed data (see Fig. 1), we investigate spatial and temporal patterns exclusively for the latter datasets. For Dataset #1, the spatial distribution of the residuals (Fig. 8a) does not show any particular spatial trends either for positive or negative between-events. From the temporal point of view, Fig. 9a shows that all the between-events of earthquakes included in Dataset #1 are within the range of ± 1 (i.e., within the uncertainty associated with macroseismic intensity) up to 1968 and between 1980 and 2005, independently of the earthquake magnitude. A positive bias is observed for most of the events that occurred in the period 1968–1980, with a general underestimation of the model with respect to the observed data (i.e., positive δBe). Conversely, the most recent earthquakes show a negative between-event, particularly after 2006. This trend could be due to the difference in the assessment of macroseismic intensity values after 1980 and after 2006 by the datasets contributing to DBMI15. In particular, in 1980 systematic collection of macroseismic data through the analysis of questionnaires compiled by local authorities (e.g. municipalities, police stations, firemen departments, etc.) began, accompanied by field surveys for the strongest earthquakes. This practice concluded at the end of 2005, and only the macroseismic field surveys following potentially damaging earthquakes have continued. Instead, intensity data of

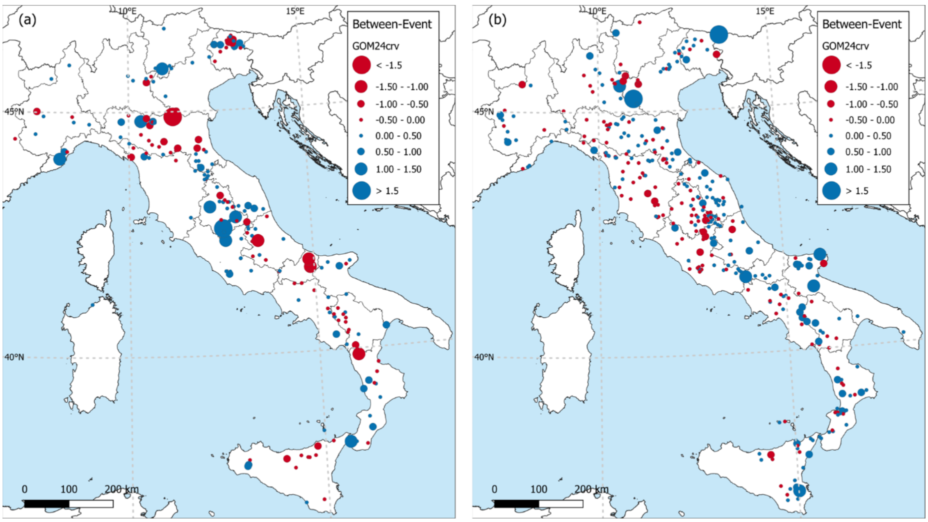

Fig. 8 Spatial distribution of the earthquakes as a function of the estimated between-event of GOM24crv contained in Dataset #1 **a** and in Dataset #2 **b**

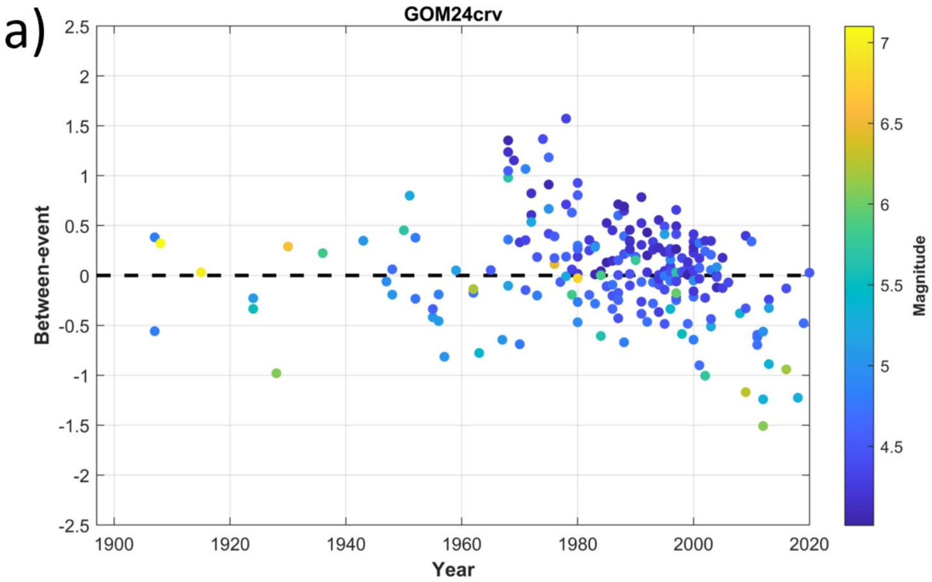

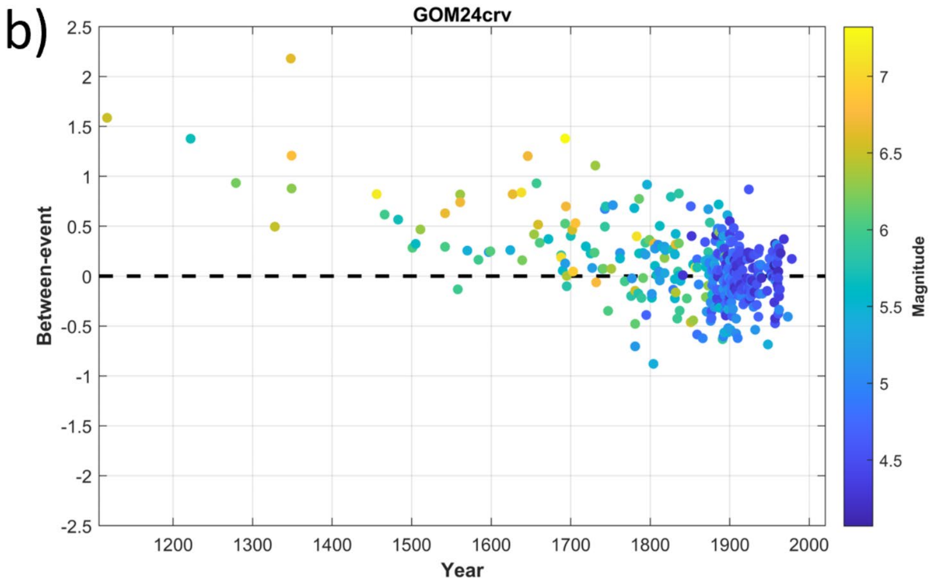

Fig. 9 Timeline of the between-event of GOM24crv of the earthquakes contained in Dataset #1 **a** and in Dataset #2 **b**

earthquakes before 1980 are mostly assessed through a posteriori analysis of contemporary documentation. Table 5 lists the earthquakes of Dataset #1 with between-events greater than or equal to ± 1. As regards the earthquakes with between-event > 1, all occurred in the period 1968–1978, and for 6 out of 8, their moment magnitude is a conversion from other types of magnitude (i.e., ISC - International Seismological Centre, Storchak et al. 2017). The highest negative between-events are observed only after 2002. In particular, the highest intensities

Table 5 Earthquakes contained in dataset #1 with between-event ≥|1| (Be_GOM24crv in decreasing order) with their date, epicentral area (area), instrumental magnitude (MwIns), and its reference (RefIns), and the number of IDPs (NIDP) with the maximum intensity (ix)

Date	Area	RefIns	MwIns	NIDP	Ix [MCS]	Be_GOM-24crv
1978 07 30	Ternano	International Seismological Centre	4.32	19	7	1.57
1974 12 02	Valnerina	Bollettino Sismico Mensile	4.43	25	8	1.37
1968 04 18	Liguria occidentale	International Seismological Centre	4.07	28	6	1.35
1968 01 04	Sabina	International Seismological Centre	4.16	12	6	1.24
1975 01 16	Stretto di Messina	International Seismological Centre	4.68	217	7–8	1.18
1969 08 11	Lago Trasimeno	International Seismological Centre	4.16	30	7	1.15
1971 07 15	Parmense	International Seismological Centre	4.9	169	8	1.07
1968 06 22	Val Lagarina	Sandron et al. (2014)	4.57	17	6	1.05
2002 10 31	Molise	Castello et al. (2006)	5.74	51	8–9	-1.00
2009 04 06	Aquilano	Bollettino Sismico Italiano	6.29	315	9–10	-1.17
2018 08 16	Molise	Bono et al. (2019)	5.29	15	5–6	-1.23
2012 10 25	Pollino	Bollettino Sismico Italiano	5.31	40	6	-1.24
2012 05 20	Pianura Emiliana	Bollettino Sismico Italiano	6.09	40	7	-1.51

Table 6 Earthquakes contained in dataset #2 with between-event ≥|1| (Be_GOM24crv in decreasing order) with their date, epicentral area (area), macroseismic magnitude (MwM), the reference of the intensity data (RefM), and the number of IDPs (NIDP) with the maximum intensity (ix)

Date	Area	RefM	MwM	NIDP	Ix [MCS]	Be_GOM24crv
1348 01 25	Alpi Giulie	Caracciolo et al. (2015)	6.63	11	9–10	2.18
1117 01 03	Veronese	Guidoboni et al. (2007)	6.52	13	9	1.59
1693 01 11	Sicilia sud-orientale	Guidoboni et al. (2007)	7.32	167	11	1.38
1222 12 25	Bresciano-Veronese	Guidoboni et al. (2007)	5.68	13	7–8	1.38
1349 09 09	Lazio-Molise	Galli and Naso (2009)	6.80	19	10–11	1.21
1646 05 31	Gargano	Camassi et al. (2008)	6.72	28	10	1.20
1731 03 20	Tavoliere delle Puglie	Guidoboni et al. (2007)	6.33	38	9	1.11

of the 6 April 2009 earthquake are not close to the instrumental epicenter (see the map in https://emidius.mi.ingv.it/CPTI15-DBMI15/), and they are hardly reproduced by isotropic IPEs (Antonucci et al. 2021). The other four earthquakes with $M_w \geq 5.3$ show a decay of their intensities faster than the model prediction following the trend shown in Fig. 5.

Concerning Dataset #2, Fig. 8b shows prevailing positive between-events but without any particular spatial trend. The timeline of the between-events represented in Fig. 9b shows a systematic underestimation (i.e., residuals > 1) of the observed intensity data by the GOM-24crv model for earthquakes in the period 1000–1746 which present very few and scattered intensity data, and macroseismic magnitudes > 5.6 (see Table 6). From 1746 to around 1900 positive between-events still prevail, and negative ones are mostly < 0.5. None of the earthquakes have between-event > -1, which means that on average the model does not significantly overestimate the observed intensities.

6 Conclusions

We test the performance of the five most recent IPEs proposed by Rovida et al. (2020), Gomez-Capera et al. (2024), and Lolli et al. (2024) for the Italian area against macroseismic data collected in DBMI15 that are associated with earthquakes with both instrumental (Dataset #1 and Dataset #1alt) and macroseismic (Dataset #2 and Dataset #2alt) parameters derived from the CPTI15 catalog. The analysis highlighted the following main findings:

- the results obtained with a diagnostic-oriented approach (analysis of residuals' trends) and measure-oriented approaches (LLH and MAE values) indicated the GOM24crv as the best-performing model. This is probably due to the different functional forms adopted with respect to the other selected IPEs (see Table 1). The GOM24crv model shows good performance for all the selected datasets.
- the statistical indexes in Table 3 show small differences, in particular for Dataset #1alt and Dataset #2alt, indicating the validity of all the tested models in reproducing on average the decay of macroseismic intensity in Italy. Such very slight differences can be attributed to the different criteria adopted for the selection of the calibration dataset of each model rather than the different attenuation models themselves.
- most of the analyzed IPEs (i.e., GOM24, ROV20, LOL24ins) tend, on average, to underestimate high-intensity values. Besides possible near-source and site effects, this might be the consequence of the use of the epicentral distance as the measure of source-to-site distance, which does not take into account the size of the rupture fault in the prediction models. However, for all the testing datasets, the GOM24crv, and LOL24all models perform better than the others with average residuals calculated for high intensities close to zero. For the LOL24 all, this could be due to the calibration dataset used for the model which includes strong earthquakes that occurred in the pre-instrumental era with a great number of high-intensity data with respect to the ones available for the instrumental earthquakes considered in the other models and for GOM24crv to the different functional form adopted;
- all the models tend to underestimate observations at long distances and overestimate those at short distances for Dataset #1, except GOM24crv; this trend is not evident for Dataset #1alt which considers also observed intensities located at distances greater than 200 km from the epicenter. For Dataset #2 and Dataset #2alt, the overestimation of observed intensities at short distances is confirmed only for the LOL24all model.
- the four models calibrated with only instrumental data (i.e., GOM24, GOM24crv, ROV20, and LOL24ins) better reproduce the observed intensities of earthquakes with instrumental location and magnitudes (Dataset #1), according to the proposed scoring. The LOL24 all model improves its performance for the two testing datasets which include macroseismic parameters (i.e., Dataset #2 and Dataset 2alt). This can be probably due to the fact that this model is calibrated considering also macroseismic locations and magnitudes. The similar behavior of the models calibrated with instrumental data when applied to different datasets proves good consistency and harmonization in the parameters of modern and historical earthquakes in the CPTI15 catalog;
- the spatial analysis of the between-event of GOM24crv does not highlight any significant regional feature of intensity attenuation in Italy, suggesting that regional IPEs might not be necessary.

In general, this study proposes a useful methodology to systematically evaluate the performance of different IPEs, borrowing the diagnostic approach adopted in the development of GMMs. Moreover, combining the results of the tests of all the models with those of the analysis of the between-event of GOM24crv, we obtain some hints for the development of future intensity attenuation models: (i) the incorporation of different distance metrics (e.g. Joyner–Boore distance) in the prediction models could allow to take into account the source effects, such as the extension of the fault. This would also avoid the isotropic decay of macroseismic intensity modelled with the common use of epicentral distance; (ii) the within-event (δW_{es}) terms could be studied in order to highlight the influence of site effects of a model prediction, as well as to verify whether propagation or rupture-directivity effects can be isolated in the intensity data.

Acknowledgements The authors wish to thank Barbara Lolli and an anonymous reviewer for their useful suggestions to improve the article.and to thank the Editor in Chief Atilla Ansal.This research is partially supported by Istituto Nazionale di Geofisica e Vulcanologia (INGV) in the frame of the project SECURE - within Pianeta Dinamico (Working Earth) - Geosciences for the Understanding of the Dynamics of the Earth and the Consequent Natural Risks (CUP code D53J19000170001), funded by the Italian Ministry of University and Research (MIUR).

Author contributions AA, GL, and AR performed the analysis. All the authors equally contributed to the analysis of the results and the writing of the final manuscript.

Data availability The event IDs of all the datasets are available in the Supplementary Information. Event parameters and macroseismic data can be retrieved through the QQuake (Locati et al. 2021), a plugin for QGIS, or via web services described and listed at: https://emidius.mi.ingv.it/ASMI/services/. DBMI15 is available at https://doi.org/10.13127/DBMI/DBMI15.4 (Locati et al. 2022). Accessed 30 Oct 2024. CPTI15 is available at https://doi.org/10.13127/CPTI/CPTI15.4 (Rovida et al. 2022b). Accessed 30 Oct 2024.

Declarations

Competing interests The authors declare that they have no conflict of interest.

References

Al Atik L, Abrahamson N, Bommer JJ, Scherbaum F, Cotton F, Kuehn N (2010) The variability of Ground-Motion Prediction models and its components. Seismol Res Lett 81:794–801. https://doi.org/10.1785/gssrl.81.5.794

Albarello D, D'Amico V (2004) Attenuation relationship of macroseismic intensity in Italy for probabilistic seismic hazard assessment. Boll Di Geofis Teor Ed Appl 45:271–284

Albarello D, D'Amico V (2005) Validation of Intensity Attenuation relationships. Bull Seismol Soc Am 95:719–724. https://doi.org/10.1785/0120040062

Albarello D, Mucciarelli M (2002) Seismic hazard estimates using Ill-defined Macroseismic Data at Site. Pure Appl Geophys 159:1289–1304. https://doi.org/10.1007/s00024-002-8682-2

Aldama-Bustos G, Douglas J, Strasser FO, Daví M, MacGregor A (2023) Methods for assessing the epistemic uncertainty captured in ground-motion models. Bull Earthq Eng 21:1–26. https://doi.org/10.1007/s10518-022-01515-8

Allen TI, Wald DJ, Worden CB (2012) Intensity attenuation for active crustal regions. J Seismol 16:409–433. https://doi.org/10.1007/s10950-012-9278-7

Antonucci A, Rovida A, D'Amico V, Albarello D (2021) Integrating macroseismic intensity distributions with a probabilistic approach: an application in Italy. Nat Hazards Earth Syst Sci 21:2299–2311. https://doi.org/10.5194/nhess-21-2299-2021

Antonucci A, Rovida A, D'Amico V, Albarello D (2023) Looking for undocumented earthquake effects: a probabilistic analysis of Italian macroseismic data. Nat Hazards Earth Syst Sci 23:1805–1816. https://doi.org/10.5194/nhess-23-1805-2023

Arroyo D, Ordaz M, Rueda R (2014) On the selection of ground-motion prediction equations for probabilistic seismic-hazard analysis. Bull Seismol Soc Am 104:1860–1875. https://doi.org/10.1785/0120130264

Azzaro R, Barbano MS, D'Amico S, Tuvè T (2006) The attenuation of seismic intensity in the Etna region and comparison with other Italian volcanic districts. Ann Geophys 49. https://doi.org/10.4401/ag-3113

Azzaro R, D'Amico S, Tuvè T (2016) Seismic hazard assessment in the volcanic region of Mt. Etna (Italy): a probabilistic approach based on macroseismic data applied to volcano-tectonic seismicity. Bull Earthq Eng 14:1813–1825. https://doi.org/10.1007/s10518-015-9806-2

Azzaro R, D'Amico S, Rotondi R, Varini E (2023) The attenuation of macroseismic intensity in the volcanic island of Ischia (Gulf of Naples, Italy): comparison between deterministic and probabilistic models and application to seismic scenarios. Bull Earthq Eng 21:5459–5479. https://doi.org/10.1007/s10518-023-01724-9

Bakun WH, Scotti O (2006) Regional intensity attenuation models for France and the estimation of magnitude and location of historical earthquakes. Geophys J Int 164:596–610. https://doi.org/10.1111/j.1365-246X.2005.02808.x

Bakun WH, Wentworth CM (1997) Estimating Earthquake Location and Magnitude from Seismic Intensity Data. Bull Seismol Soc Am 87:1502–1521. https://doi.org/10.1785/BSSA0870061502

Baumont D, Manchuel K, Traversa P, Durouchoux C, Nayman E, Ameri G (2018) Intensity predictive attenuation models calibrated in Mw for metropolitan France. Bull Earthq Eng 16:2285–2310. https://doi.org/10.1007/s10518-018-0344-6

Bayrak E, Nas M, Bayrak Y (2019) New macroseismic intensity predictive models for Turkey. Acta Geophys 67:1483–1513. https://doi.org/10.1007/s11600-019-00357-4

Bindi D, Parolai S, Oth A, Abdrakhmatov K, Muraliev A, Zschau J (2011) Intensity prediction equations for Central Asia: intensity attenuation model for Central Asia. Geophys J Int 187:327–337. https://doi.org/10.1111/j.1365-246X.2011.05142.x

Bollettino Sismico Mensile Istituto Nazionale di Geofisica (ING)

Bollettino Sismico Italiano (2024) Istituto Nazionale di Geofisica e Vulcanologia (INGV), http://bollettinosismico.rm.ingv.it/. Accessed 30

Bono A, Lombardi AM, Rossi A, Nardi A, Marchetti A, Improta L, Berardi M, Latorre D, Mele FM, Margheriti L, Battelli P (2019) Bollettino Sismico Italiano (BSI), II quadrimestre 2018 (Version 1), Istituto Nazionale di Geofisica e Vulcanologia (INGV). https://doi.org/10.13127/BSI/201802. Accessed 30 Oct 2024

BRGM-EDF-IRSN/SisFrance (2014) Histoire et caractéristiques des séismes ressentis en France. http://www.sisfrance.net/. Accessed 30 Oct 2024

Camassi R, Bernardini F, Castelli V, Meletti C (2008) A 17th Century Destructive Seismic Crisis in the Gargano Area: its implications on the understanding of local seismicity. J Earthq Eng 12:1223–1245. https://doi.org/10.1080/13632460802212774

Caracciolo CH, Camassi R, Castelli V (2015) Il terremoto del 25 gennaio 1348 (Alpi Orientali). Rapporto interno, 12pp edn. Istituto Nazionale di Geofisica e Vulcanologia

Castellaro S, Mulargia F, Kagan YY (2006) Regression problems for magnitudes. Geophys J Int 165:913–930. https://doi.org/10.1111/j.1365-246X.2006.02955.x

Castello B, Selvaggi G, Chiarabba C, Amato A (2006) CSI Catalogo della sismicità italiana 1981–2002, versione 1.1. https://doi.org/10.13127/CSI.1.1. Istituto Nazionale di Geofisica e Vulcanologia (INGV)

Cito P, Chioccarelli E, Iervolino I (2022) Macroseismic intensity hazard maps for Italy based on a recent grid source model. Bull Earthq Eng 20:2245–2258. https://doi.org/10.1007/s10518-022-01323-0

Cotton F, Scherbaum F, Bommer JJ, Bungum H (2006) Criteria for selecting and adjusting ground-motion models for specific target regions: application to central Europe and rock sites. J Seismol 10:2, 137–156. https://doi.org/10.1007/s10950-005-9006-7

D'Amico V, Albarello D (2008) SASHA: A Computer Program to assess seismic hazard from Intensity Data. Seismol Res Lett 79:663–671. https://doi.org/10.1785/gssrl.79.5.663

D'Amico V, Visini F, Rovida A, Marzocchi W, Meletti C (2024) Scoring and ranking probabilistic seismic hazard models: an application based on macroseismic intensity data. Nat Hazards Earth Syst Sci Discuss. https://doi.org/10.5194/nhess-2023-203

Delavaud E, Cotton F, Akkar S, Scherbaum F, Danciu L, Beauval C, Drouet S, Douglas J, Basili R, Sandikkaya M, Segou M, Faccioli E, Theodoulidis N (2012) Toward a ground-motion logic tree for probabilistic seismic hazard assessment in Europe. J Seismol 16:451–473. https://doi.org/10.1007/s10950-012-9281-z

Drouet S, Ameri G, Le Dortz K, Secanell R, Senfaute G (2020) A probabilistic seismic hazard map for the metropolitan France. Bull Earthq Eng 18:1865–1898. https://doi.org/10.1007/s10518-020-00790-7

Fuller WA (ed) (1987) Measurement error models. John Wiley & Sons, Inc., Hoboken, NJ, USA

Galli P, Naso JA (2009) Unmasking the 1349 earthquake source (southern Italy): paleoseismological and archaeoseismological indications from the Aquae Iuliae fault. J Struct Geol 31:128–149. https://doi.org/10.1016/j.jsg.2008.09.007

Gardner JK, Knopoff L (1974) Is the sequence of earthquakes in Southern California, with aftershocks removed. Poissonian? Bull Seismol Soc Am 64:1363–1367. https://doi.org/10.1785/BSSA0640051363

Gasperini P (2001) The attenuation of seismic intensity in Italy: a bilinear shape indicates the dominance of deep phases at Epicentral Distances Longer than 45 km. Bull Seismol Soc Am 91:826–841. https://doi.org/10.1785/0120000066

Gasperini P, Bernardini F, Valensise G, Boschi E (1999) Defining Seismogenic sources from historical earthquake Felt Reports. Bull Seismol Soc Am 89:94–110. https://doi.org/10.1785/BSSA0890010094

Gasperini P, Vannucci G, Tripone D, Boschi E (2010) The location and sizing of historical earthquakes using the attenuation of Macroseismic Intensity with Distance. Bull Seismol Soc Am 100:2035–2066. https://doi.org/10.1785/0120090330

Gomez-Capera A (2006) Seismic hazard map for the Italian territory using macroseismic data. Earth Sci Res J 10:67–90

Gomez-Capera AA, D'Amico V, Meletti C, Rovida A, Albarello D (2010) Seismic Hazard Assessment in terms of Macroseismic Intensity in Italy: a critical analysis from the comparison of different computational procedures. Bull Seismol Soc Am 100:1614–1631. https://doi.org/10.1785/0120090212

Gomez-Capera AA, Santulin M, D'Amico M, D'Amico V, Locati M, Meletti C, Varini E (2024) Macroseismic intensity attenuation models calibrated in Mw for Italy. Bull Earthq Eng. https://doi.org/10.1007/s10518-023-01822-8

Goulet C, Bozorgnia Y, Kuehn N, Al Atik L, Youngs R, Graves R, Atkinson G (2017) NGA-East Ground-Motion models for the U.S. Geological Survey National Seismic Hazard maps (PEER Reports), PEER Reports. Pacific Earthquake Engineering Research Center, University of California, Berkeley, CA. https://doi.org/10.55461/QOZJ4825

Gruppo di lavoro CPTI (2004) Catalogo Parametrico dei Terremoti Italiani (CPTI04). Istituto Nazionale di Geofisica e Vulcanologia (INGV), Bologna. https://doi.org/10.6092/INGV.IT-CPTI04. Accessed 30 Oct 2024

Guidoboni E, Ferrari G, Mariotti D, Comastri A, Tarabusi G, Valensise G (2007) CFTI4Med, Catalogue of Strong Earthquakes in Italy (461 B.C.-1997) and Mediterranean Area (760 B.C.-1500). INGV-SGA. https://storing.ingv.it/cfti/cfti4/# Accessed 30 Oct 2024

Gupta IN, Nuttli OW (1976) Spatial attenuation of intensities for central U.S. earthquakes. Bull Seismol Soc Am 66:743–751. https://doi.org/10.1785/BSSA0660030743

Howell BF, Schultz TR (1975) Attenuation of modified mercalli intensity with distance from the epicenter. Bull Seismol Soc Amer 65(3):651–665. https://doi.org/10.1785/BSSA0650030651

Kale O, Akkar S (2013) A New Procedure for selecting and ranking ground-motion prediction equations (GMPEs): the Euclidean Distance-based ranking (EDR) method. Bull Seismol Soc Am 103:1069–1084. https://doi.org/10.1785/0120120134

Kövesligethy R (1907) Seismischer Stärkegrad Und Intensität Der Beben, Gerlands Beitr. Zur Geophys 8:21–103 (in German)

Lanzano G, Luzi L, D'Amico V, Pacor F, Meletti C, Marzocchi W, Rotondi R, Varini E (2020) Ground motion models for the new seismic hazard model of Italy (MPS19): selection for active shallow crustal regions and subduction zones. Bull Earthq Eng 18:3487–3516. https://doi.org/10.1007/s10518-020-00850-y

Locati M, Vallone R, Ghetta M, Dawson N (2021) QQuake, a QGIS Plugin for Loading Seismological Data from Web Services. Front Earth Sci. https://doi.org/10.3389/feart.2021.614

Locati M, Camassi R, Rovida A, Ercolani E, Bernardini F, Castelli V, Caracciolo CH, Tertulliani A, Rossi A, Azzaro R, D'Amico S, Antonucci A (2022) Database Macrosismico Italiano (DBMI15), versione 4.0. Istituto Nazionale di Geofisica e Vulcanologia (INGV). https://doi.org/10.13127/DBMI/DBMI15.4. Accessed 30 Oct 2024

Lolli B, Gasperini P, Vannucci G (2024) Recalibration of the intensity prediction equation in Italy using the macroseismic dataset DBMI15 version 2.0. Seismol Res Lett. https://doi.org/10.1785/0220230212

Mak S, Clements RA, Schorlemmer D (2015) Validating intensity prediction equations for Italy by observations. Bull Seismol Soc Am 105:2942–2954. https://doi.org/10.1785/0120150070

Manchuel K, Traversa P, Baumont D, Cara M, Nayman E, Durouchoux C (2018) The French seismic CATalogue (FCAT-17). Bull Earthq Eng 16:2227–2251. https://doi.org/10.1007/s10518-017-0236-1

Meletti C, Marzocchi W, D'Amico V, Lanzano G, Luzi L, Martinelli F, Pace B, Rovida A, Taroni M, Visini F (2021) The new Italian seismic hazard model (MPS19). Ann Geophys 64:6. https://doi.org/10.4401/ag-8579

Musson RMW (2013) Updated intensity attenuation for the UK. British Geological Survey. Earth Hazards and Systems Programme, open report

Oliveti I, Faenza L, Antonucci A, Locati M, Rovida A, Michelini A (2023) The ShakeMap Atlas of historical earthquakes in Italy: configuration and validation. Seismol Res Lett. https://doi.org/10.1785/0220230138

Pasolini C, Gasperini P, Albarello D, Lolli B, D'Amico V (2008a) The attenuation of seismic intensity in Italy, Part I: theoretical and empirical backgrounds. Bull Seismol Soc Am 98:682–691. https://doi.org/10.1785/0120070020

Pasolini C, Albarello D, Gasperini P, D'Amico V, Lolli B (2008b) The attenuation of seismic intensity in Italy, Part II: modeling and validation. Bull Seismol Soc Am 98:692–708. https://doi.org/10.1785/0120070021

Provost L, Scotti O (2020) QUake-MD: open-source code to quantify uncertainties in magnitude–depth estimates of earthquakes from Macroseismic Intensities. Seismol Res Lett 91:2520–2530. https://doi.org/10.1785/0220200064

Rey J, Beauval C, Douglas J (2018) Do French macroseismic intensity observations agree with expectations from the European seismic hazard model. 2013? J Seismol 22:589–604. https://doi.org/10.1007/s10950-017-9724-7

Rotondi R, Varini E (2019) Prodotto 4.9: Aggiornamento dei modelli probabilistici di attenuazione in funzione di I0. In: Meletti, C. e Marzocchi, W. (a cura di), Il modello di pericolosità sismica MPS19, rapporto finale, Centro Pericolosità Sismica, Istituto Nazionale di Geofisica e Vulcanologia, maggio 2019, Roma, 168

Rotondi R, Varini E, Brambilla C (2016) Probabilistic modelling of macroseismic attenuation and forecast of damage scenarios. Bull Earthq Eng 14:1777–1796. https://doi.org/10.1007/s10518-015-9781-7

Rovida A, Locati M, Camassi R, Lolli B, Gasperini P (2020) The Italian earthquake catalogue CPTI15. Bull Earthq Eng 18:2953–2984. https://doi.org/10.1007/s10518-020-00818-y

Rovida A, Antonucci A, Locati M (2022a) The European Preinstrumental Earthquake Catalogue EPICA, the 1000–1899 catalogue for the European seismic hazard model 2020. Earth Syst Sci Data 14:5213–5231. https://doi.org/10.5194/essd-14-5213-2022

Rovida A, Locati M, Camassi R, Lolli B, Gasperini P, Antonucci A (2022b) Italian Parametric Earthquake Catalogue (CPTI15), version 4.0. Istituto Nazionale di Geofisica e Vulcanologia (INGV). https://doi.org/10.13127/CPTI/CPTI15.4. Accessed 30 Oct 2024

Sammon JW (1969) A nonlinear mapping for data structure analysis. IEEE Trans Comput 18(5):401–409. https://doi.org/10.1109/t-c.1969.222678

Sandron D, Renner G, Rebez A, Slejko D (2014) Early instrumental seismicity recorded in the eastern Alps. Bollettino Di Geofis Teorica Ed Appl 55:755–788. https://doi.org/10.4430/bgta0118

Scherbaum F, Delavaud E, Riggelsen C (2009) Model selection in seismic hazard analysis: an information-theoretic perspective. Bull Seismol Soc Am 99:3234–3247. https://doi.org/10.1785/0120080347

Scherbaum F, Kuehn NM, Ohrnberger M, Koehler A (2010) Exploring the proximity of Ground-Motion models using high-dimensional visualization techniques. Earthq Spectra 26:1117–1138. https://doi.org/10.1193/1.3478697

Sieberg A (1923) Geologische, physikalische und angewandte Erdbebenkunde. G. Fischer, Jena

Sørensen MB, Stromeyer D, Grunthal G (2009) Attenuation of macroseismic intensity: a New Relation for the Marmara Sea Region, Northwest Turkey. Bull Seismol Soc Am 99:538–553. https://doi.org/10.1785/0120080299

Sørensen MB, Stromeyer D, Grünthal G (2010) A macroseismic intensity prediction equation for intermediate depth earthquakes in the Vrancea region. Romania Soil Dynamics Earthq Eng 30:1268–1278. https://doi.org/10.1016/j.soildyn.2010.05.009

Stafford PJ (2014) Crossed and nested mixed-effects approaches for enhanced Model Development and removal of the Ergodic Assumption in empirical ground-motion models. Bull Seismol Soc Am 104:702–719. https://doi.org/10.1785/0120130145

Storchak DA, Harris J, Brown L, Lieser K, Shumba B, Verney R, Di Giacomo D, Korger EIM (2017) Rebuild of the Bulletin of the International Seismological Centre (ISC), part 1: 1964–1979. Geosci Lett 4:32. https://doi.org/10.1186/s40562-017-0098-z

Stromeyer D, Grunthal G (2009) Attenuation relationship of macroseismic intensities in Central Europe. Bull Seismol Soc Am 99:554–565. https://doi.org/10.1785/0120080011

Tosi P, Sbarra P, De Rubeis V, Ferrari C (2015) Macroseismic Intensity Assessment Method for web questionnaires. Seismol Res Lett 86:985–990. https://doi.org/10.1785/0220140229

Publisher's note Springer Nature remains neutral with regard to jurisdictional claims in published maps and institutional affiliations.